Energy & Environmental Science

PAPER

View Article Online
View Journal | View Issue

Cite this: *Energy Environ. Sci.*, 2014, **7**, 760

A fast, inexpensive method for predicting overcharge performance in lithium-ion batteries†

Susan A. Odom,* Selin Ergun, Pramod P. Poudel and Sean R. Parkin

Received 9th July 2013
Accepted 8th November 2013

DOI: 10.1039/c3ee42305k

www.rsc.org/ees

A variety of mechanisms lead to the failure of lithium-ion batteries. One is overcharge, a condition in which a battery's voltage rises above its designed end-of-charge potential. Electrolyte additives called redox shuttles limit cell potential by preferentially oxidizing, and cycling between the cathode and anode in their radical cation and neutral forms. Currently, testing requires coin cell assembly and repeated cycling, which can be an expensive and time consuming process. It is commonly accepted that degradation of the radical cation form of a redox shuttle leads to overcharge protection failure. We thus studied the stability of the radical cation forms of a series of redox shuttle additives to determine if there is a correlation between radical cation stability and the number of cycles of overcharge protection. While the reversibility of oxidations in cyclic voltammetry did not correlate to trends in overcharge performance, results from both UV-vis and electron paramagnetic resonance spectroscopy showed a correlation between stability and overcharge protection. Our results reveal trends within a few hours for what otherwise takes months of battery cycling to determine, providing a fast and relatively inexpensive method for predicting redox shuttle performance.

Broader context

Hundreds of compounds have been tested as redox shuttles for lithium-ion batteries, but only a small percent of compounds have resulted in overcharge protection for more than a few cycles. For this area of research to progress, it is necessary to identify faster, less expensive screening methods of redox shuttle candidates. From published protocols, a typical overcharge cycle takes about 20 h, and for the most robust redox shuttles can take weeks or months of cycling before failure. Additionally, the equipment required to assemble and cycle batteries is extensive and costly. Using UV-vis spectroscopy of radical cations enables a small amount of analyte to be studied, and our results show clear trends in radical cation stability in a few hours, despite significant differences in concentration (3×10^{-4} M *vs.* 0.1 M) and solvent environment (dichloromethane *vs.* carbonate solvents with lithium salts). We plan to use this method to identify potential redox shuttle candidates prior to battery cycling.

I. Introduction

Lithium-ion batteries (LIBs) are ubiquitous in consumer electronics[1,2] and have been commercialized for hybrid vehicles and commercial aircraft.[1,3,4] Despite wide commercial use, safety concerns and limited lifetimes have restricted the development of large-scale LIBs.[4–7] A common safety issue in LIBs is overcharge, a condition in which charging current is applied to a battery that has reached its end-of-charge potential, raising cell potential to undesirably high values.[4,8] This situation leads to an excess of lithium deintercalation, which may cause irreversible phase transitions in the cathode,[9] as well as oxidation and reduction reactions at the cathode/electrolyte surface, leading to electrolyte decomposition and gas production.[10–12] Increased internal pressure may pose safety hazards, and heat generated from these reactions may lead to thermal runaway conditions, increasing the risk of fires and explosions. To prevent overcharge in LIBs, electrolyte additives called redox shuttles have been utilized to limit cell voltage. Redox shuttles prevent overcharge by oxidizing at the cathode, then shuttling to anode where they are reduced to their neutral form, thus mitigating excess current and stabilizing cell voltage.[4,8] Of the two forms of redox shuttle present during overcharge, the stability of the more reactive radical cation form of the redox shuttle is a critical factor for longevity.

Overcharge protection in LIBs has been demonstrated with a variety of redox shuttles.[4,8] The majority of shuttles relevant to 4 V or higher LIBs consist of aromatic compounds, organometallic compounds,[13–28] and conjugated polymers.[29–33] Radicals[34,35] and inorganic salts[21,36–39] have also been used to demonstrate overcharge protection. Redox shuttle performance is usually measured by the number of overcharge cycles in which voltage stabilization is achieved, given a defined amount

Department of Chemistry, University of Kentucky, Chemistry-Physics Building, Lexington, KY, USA. E-mail: susan.odom@uky.edu; Fax: +1 001 859 323 1069; Tel: +1001 859 257 3294

† Electronic supplementary information (ESI) available. CCDC 949271. For ESI and crystallographic data in CIF or other electronic format see DOI: 10.1039/c3ee42305k

of excess charging current. Overcharge performance is affected by redox shuttle solubility, diffusion coefficient, and chemical stability of the neutral and oxidized (radical cation) forms. Solubility in battery electrolytes can be predicted by the composition and placement of polar, nonpolar, hydrogen-bonding, and aromatic components. Diffusion coefficients can be estimated by the size and shape of a molecule. However, predicting the relative stability of redox shuttles is a more difficult task, especially in the radical cation (oxidized) form. Radical cations are more reactive than their neutral counterparts due to their electron deficiency and radical nature. These species undergo a variety of substitution reactions with nucleophiles[40,41] as well as dimerization and polymerization reactions.[42–44] While DFT calculations have been used to explain stability and to propose decomposition pathways of radical cations,[25,28,45,46] no studies have been reported that predict the performance of untested redox shuttle candidates.

In addition to the lack of predictive methods in redox shuttle performance, no methods have been identified to screen redox shuttle candidates prior to battery assembly and cycling. Thus new compounds must be tested in batteries to determine overcharge performance: a costly and lengthy process. An argon-filled glove box, coin cell supplies, coin cell crimper, and battery cycler easily total $100k for a basic setup. Additionally, a significant amount of time may be required to obtain cycling results. If a redox shuttle additive fails to go beyond a few overcharge cycles, the experiment is finished within a few days. However, if a redox shuttle is effective in overcharge protection, cycling may require weeks or months to complete. As redox shuttle design improves, rigorous testing by current methods could require years of cycling before failure.

A fast, inexpensive approach is needed for more efficient screening of potential redox shuttles to identify promising candidates for overcharge protection. Such a method could be used to limit battery cycling to only the more promising candidates, thus saving time and money when less viable candidates are eliminated. Because the radical cations of aromatic compounds are more reactive than their neutral counterparts, we examined the stability of these oxidized species. We predicted that the stability of radical cations could be used to determine redox shuttle performance: a more stable radical cation should correlate to a redox shuttle with a larger number of overcharge protection cycles. While it is generally accepted that radical cation stability is a key factor in redox shuttle performance, there have been no experimental studies that have shown whether radical cation stability correlates with redox shuttle performance.

A variety of analytical techniques can be used to study radical cation species. For example, Dahn and coworkers used UV-vis absorption spectra to analyze radical cations of the redox shuttle 1,4-bis(*tert*-butyl)-2,5-dimethoxybenzene, although their study did not focus on lifetimes.[47] Our previous work in the spectroscopic analysis of radical cations inspired us to use transient UV-vis absorption and electron paramagnetic resonance (EPR) spectroscopy to measure the stability of radical cations. We selected UV-vis because of its simplicity and EPR because of its unambiguous identification of radical species.

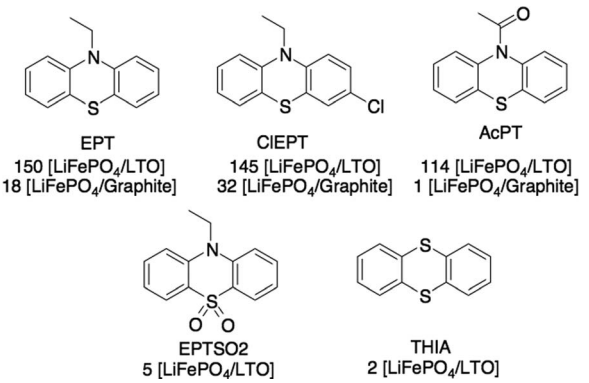

Fig. 1 Fused-ring heteroaromatic redox shuttles reported for overcharge protection and the number of cycles reported with relevant electrodes.[17,18,45]

Given the large number of compounds tested as redox shuttles, we limited initial experiments to a group of structurally similar redox shuttles reported by the same laboratory, specifically the Dahn group. The compounds studied include *N*-ethylphenothiazine and similarly structured anthracene-based heterocycles (Fig. 1).[17,18,45] Herein we present the results of radical cation stability measurements using UV-vis and EPR spectroscopy compared with the number of overcharge protection cycles reported for the corresponding redox shuttles.

II. Experimental section

General

3-Chloro-*N*-ethylphenothiazine (ClEPT), *N*-acetylphenothiazine (AcPT), *N*-ethylphenothiazine-(*S*,*S*)-dioxide (EPTSO2), and thianthrene (THIA) were purchased from Sigma Aldrich and were used without further purification. *N*-Ethylphenothiazine was synthesized in our laboratory, following a similar procedure for the previously reported compound.[48] The chemical oxidant tris(2,4-dibromophenyl)aminium hexachloroantimonate (TDBPA$^{\bullet+}$ or Magic Green)[49] and its neutral precursor were synthesized in our laboratory. Sodium hydride was purchased from Alfa Aesar, bromine and bromoethane from Sigma Aldrich, and antimony pentachloride from Acros Organics. Silica gel (65 × 250 mesh) was purchased from Sorbent Technologies, and solvents for product purification were purchased from Fisher Scientific. Ethylene carbonate, ethyl methyl carbonate, and lithium hexafluorophosphate were purchased from BASF Corporation (NJ, USA). ^{1}H and ^{13}C NMR spectra were obtained on Varian spectrometers in DMSO-d_6 or $CDCl_3$ from Cambridge Isotope Laboratories. Mass spectra were obtained on an Agilent 5973 Network mass selective detector attached to Agilent 6890N Network GC system. Elemental analyses were performed by Atlantic Microlabs.

Synthesis of *N*-ethylphenothiazine (EPT)

Sodium hydride (4.8 g, 110 mmol, 60% dispersion in mineral oil) was added to a solution of phenothiazine (19.9 g, 100 mmol) in anhydrous *N*,*N*-dimethylformamide (100 mL) in a 250 mL

round-bottomed flask under nitrogen atmosphere. The reaction flask was immersed in an oil bath, which was heated to 50 °C for 20 min. A reflux condenser was attached, and ethylbromide (12.0 g, 110 mmol) was added dropwise to the reaction mixture through the condenser and was stirred overnight. Water (500 mL) was added, and the organic product was extracted with hexanes (2 × 300 mL). The combined organic layers were dried over $MgSO_4$ and were concentrated by rotary evaporation. The crude product was purified by recrystallization from ethanol, yielding the product (20.1 g, 90%) as a white solid. ^{1}H NMR (400 MHz, DMSO-d_6) δ (ppm): 7.21–7.17 (m, 2H), 7.13 (dd, J = 7.6, 1.6 Hz, 2H), 7.00 (dd, J = 8.2, 1.0 Hz, 2H), 6.92 (td, J = 7.5, 1.2 Hz, 2H), 3.9 (q, J = 6.9 Hz, 2H), 1.3 (t, J = 6.9 Hz, 3H). ^{13}C NMR (100 MHz, DMSO-d_6) δ (ppm): 144.40, 127.57, 126.98, 122.97, 122.33, 115.43, 40.98, 12.66. GCMS: m/z 227 (50%), 212 (10%), 198 (100%), 167 (13%). Anal. calcd for $C_{14}H_{13}SN$ C, 73.97; H, 5.76; N, 6.16 . Found C, 73.91; H, 5.87; N, 6.12 and C, 73.72; H, 5.82; N, 6.16%.

Synthesis of tris-(2,4-dibromophenyl)amine

Triphenylamine (0.491 g, 2.00 mmol) was added to an oven-dried 50 mL round-bottomed flask cooled under nitrogen. Anhydrous dichloromethane (10 mL) was added to the reaction flask, after which bromine (1.92 g, 12.0 mmol) in dichloromethane (2 mL) was added dropwise. The reaction mixture was stirred at r.t., with monitoring by GCMS. Additional bromine (0.36 g, 2.3 mmol at 27 h and 0.16 g, 1.0 mmol at 44 h) was added to the reaction flask followed by dichloromethane (100 mL) after 48 h total reaction time. The organic layer was washed with aq. $Na_2S_2O_3$, and was dried over $MgSO_4$, filtered, and concentrated by rotary evaporation, resulting in a white solid. The product was purified by crystallization in a 3 : 1 solution of dichloromethane:ethanol, which was allowed to evaporate slowly at r.t. Filteration yielded the product as a colorless crystalline solid (0.89 g, 62%). ^{1}H NMR (400 MHz, $CDCl_3$) δ 7.73 (d, J = 2.4, 3H), 7.33 (dd, J = 2.4, 8.4, 3H), 6.67 (d, J = 8.4, 3H). ^{13}C NMR (100 MHz, $CDCl_3$) δ 144.3, 137.3, 131.5, 128.1, 122.3, 118.7. MS (EI) m/z 719 [M^+]. Anal. calcd for $C_{18}H_9Br_6N$: C, 30.08; H, 1.26; N, 1.95. Found: C, 30.22; H, 1.12; N, 2.02%. Atomic connectivity was confirmed by single crystal X-ray analysis (Fig. S1†).

Synthesis of tris-(2,4-dibromophenyl)aminium hexachloroantimonate (TDBPA$^{\bullet+}$)

Tris-(2,4-dibromophenyl)amine (0.18 g, 0.25 mmol) was added to a 100 mL oven-dried round-bottomed flask cooled under nitrogen. Anhydrous dichloromethane (15 mL) was added to the flask, which was capped with a rubber septum, immersed in an ice water bath, and purged with nitrogen. Dropwise addition of antimony pentachloride (48 μL, 0.11 g, 0.38 mmol) to the reaction mixture produced a dark green solution, which was stirred for 10 min. The reaction mixture was then cooled to −20 °C, and anhydrous hexanes (60 mL) were added, resulting in the formation of a green precipitate, which was filtered and washed with anhydrous hexanes (15 mL). The title compound was obtained as a green solid (0.26 g, 99%), which was transferred to an argon-filled glove box for long-term storage immediately after isolation. An EPR spectrum of the product (Fig. S2†) showed that a radical is present. UV-vis absorption spectra showed a broad band centered at *ca.* 860 nm (Fig. S3†).

Cyclic voltammetry

Cyclic voltammetry (CV) experiments were performed using a CH Instruments 600D potentiostat. The electrolyte consisted of 0.1 M nBu$_4$NPF$_6$ in dichloromethane (DCM) and contained *ca.* 3 × 10^{-4} M analyte. Glassy carbon was used as the working electrode, platinum as the counter electrode, and freshly anodized silver/silver chloride as the reference electrode. Decamethylferrocene (Cp*$_2$Fe, $E_{1/2}^{+/0}$ = −0.55 V *vs.* $Cp_2Fe^{+/0}$ at 0 V) was added to each sample as an internal reference. Voltammograms were recorded at scan rates of 100 mV s^{-1}, and multiple scans were performed for each sample to assure reproducibility.

UV-vis and EPR spectroscopy

UV-vis spectra were obtained using optical glass cuvettes (Starna) on an Agilent 8453 diode array spectrometer. The analyte (0.009 mmol, 2–3 mg) was dissolved in anhydrous dichloromethane (2.9 mL) in a vial and was transferred to a cuvette with a 10 mm path length. A freshly prepared solution of TDBPA$^{\bullet+}$ oxidant (100 μL, 9.0 × 10^{-3} M in dichloromethane) was added using a Hamilton syringe, and the cuvette was immediately capped with a teflon stopper and rotated to distribute the oxidant throughout the sample. Assuming complete electron transfer, this reaction yields a net concentration of 3.0 × 10^{-4} M radical cation, 3.0 × 10^{-4} M neutral form of the oxidizing agent, and 2.7 × 10^{-3} M unreacted, neutral redox shuttle remains. Numerous spectra were obtained at various times from the initial spectra up to 10 h. For EPR studies, the same amounts and concentrations of neutral redox shuttle and oxidant were combined and transferred to a 4 mm quartz EPR tube (Wilmad). Spectra were collected on an X-band Bruker EPR spectrometer. In both UV-vis and EPR experiments, all solutions of oxidant were used within 10 min of preparation to minimize oxidant decomposition, and the initial spectra were acquired within 1 min of oxidant addition for UV-vis samples and within 5 min for EPR samples.

III. Results and discussion

Radical cations can be generated by a variety of techniques, including bulk electrolysis, irradiation with gamma rays, and reaction with a chemical oxidant. Striving for simplicity in the experimental setup, we used a chemical oxidant to generate radical cations. In order to identify an appropriate chemical oxidant to produce radical cations of EPT and related redox shuttles, CV was used to determine oxidation potentials. Our electrolyte contained the solvent dichloromethane (DCM) and 0.1 M nBu$_4$NPF$_6$; we preferred DCM as the solvent for UV-vis and EPR studies due to its low cost, ability to solubilize aromatic compounds, lack of strong nucleophilic components, and naturally anhydrous nature. Additionally, it is not possible to

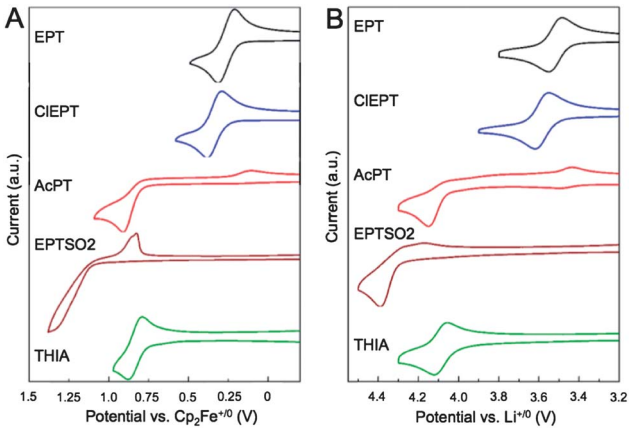

Fig. 2 Cyclic voltammograms of EPT (black), ClEPT (blue), AcPT (red), EPTSO2 (maroon), and THIA (green) in 0.1 M nBu$_4$NPF$_6$ in dichloromethane (left) and in 1.2 M LiPF$_6$ in EC/EMC (right) recorded at a scan rate of 100 mV s^{-1}. Potentials in dichloromethane are referenced to CpFe$^{+/0}$ at 0 V, and those in EC/EMC are referenced to Li$^{+/0}$ at 0 V.

acquire EPR spectra in standard 4 mm tubes with the typical carbonates used in battery electrolytes at r.t. because these solvents are too polar to allow for tuning of the EPR cavity. For comparison with a common LIB electrolyte, we recorded voltammograms in Argonne National Laboratory's "generation 2" battery electrolyte: ethylene carbonate/ethyl methyl carbonate (3 : 7) containing 1.2 M LiPF$_6$. The voltammograms recorded in 0.1 M nBu$_4$NPF$_6$ in DCM were referenced to Cp$_2$Fe$^{+/0}$ at 0 V, and the voltammograms recorded in 1.2 M LiPF$_6$ in EC/EMC were referenced to Li$^{+/0}$ at 0 V. The voltammograms from both solvent systems are shown in Fig. 2, excluding the portion of the voltammograms containing the oxidation of the internal standard (see Fig. S4† for the complete voltammograms). The oxidation potentials in both electrolytes, which were calculated by averaging the peaks of the forward and reverse waves, are reported in Table 1. In the case of irreversible oxidations (AcPT and EPTSO2), oxidation potentials were calculated by averaging the oxidation peak and an estimate of where the reduction peak would have occurred if the oxidation had been reversible; therefore these values may not be as reliable.

In a chemical oxidation reaction, the chemical oxidant accepts an electron from its neutral counterpart, thus

Table 1 Oxidation potentials ($E_{1/2}^{+/0}$) of EPT, ClEPT, AcPT, EPTSO2, and THIA in 0.1 M nBu$_4$NPF$_6$ in DCM *vs.* Cp$_2$Fe$^{+/0}$ at 0 V and in 1.2 M LiPF$_6$ in EC/EMC *vs.* Li$^{+/0}$ at 0 V

Compound	$E_{1/2}^{+/0}$ *vs.* Cp$_2$Fe$^{+/0}$ (V)	$E_{1/2}^{+/0}$ *vs.* Li$^{+/0}$ (V)
EPT	0.26	3.52
ClEPT	0.34	3.58
AcPT[a]	0.85[c]	4.08[c]
AcPT[b]	0.14	3.42
EPTSO2	1.18[c]	4.34[c]
THIA	0.84	4.09

[a] Original peak. [b] Peak that appeared in subsequent scans. [c] Oxidation was not reversible.

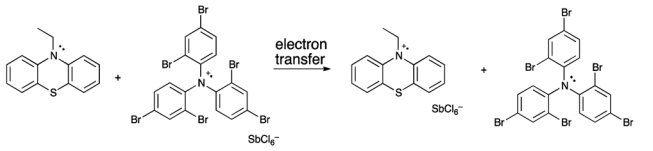

Scheme 1 Representation of the electron transfer reaction of EPT with TDBPA$^{\bullet+}$ in which the radical cation of EPT and the neutral form of the triarylamine derivative are produced.[51]

generating the radical cation of the redox shuttle (Scheme 1). In order to use the same chemical oxidant for this series of compounds, it is necessary that the oxidation potential of the neutral version of the chemical oxidant occurs at a higher potential than that of all of the neutral compounds in the series. The shape of the oxidation of EPTSO2 is quite far from reversible, so our estimate of 1.18 V for the oxidation has an unknown yet possibly large error. Therefore we neglected its estimated potential in the identification of an appropriate oxidizing agent. Although we had hoped that the commercially available oxidant tris(4-bromophenyl)aminium hexachloroantimonate (TBPA$^{\bullet+}$, known as Magic Blue) would be compatible with the series, the oxidation potentials of AcPT and THIA of 0.85 and 0.84 V, respectively, *vs.* Cp$_2$Fe$^{+/0}$ are not low enough to undergo an electron transfer reaction with TBPA$^{\bullet+}$, as the oxidation potential of the neutral form of TBPA$^{\bullet+}$, tris(4-bromophenyl)amine, is 0.70 V *vs.* Cp$_2$Fe$^{+/0}$. A related oxidant tris(2,4-dibromophenyl)-aminium hexachloroantimonate (TDBPA$^{\bullet+}$, also known as Magic Green), for which the oxidation potential of its neutral form is 1.1 V *vs.* Cp$_2$Fe$^{+/0}$, is compatible with the oxidation potentials of the compounds in this series. This oxidant can be synthesized in two steps from triphenylamine.[49,50]

From the CV experiments we found that the reversibility of the oxidations does not correlate to overcharge performance, and therefore, CV cannot be used as a reliable screening method for redox shuttle performance. AcPT, which undergoes overcharge protection for a relatively high number of overcharge cycles (114), has an irreversible oxidation in both electrolytes, and would not be expected to be an effective redox shuttle. Also, THIA, which limits battery potential for only two overcharge cycles, displays a reversible oxidation in both electrolytes. The time scale of the CV experiment can be used to explain why a relatively poor redox shuttle like THIA displays a reversible oxidation: the time from the start of the oxidation of THIA until its return to neutral is about 8 seconds, which is orders of magnitude shorter than one cycle of overcharge protection (often ~20 h). A radical cation that is stable for 8 s cannot be guaranteed to last even one overcharge cycle.

The case of AcPT is more interesting as one would expect that a radical cation that decomposed in less than 8 s would not demonstrate any overcharge protection. However, with AcPT, this is not the case. Notice, though, that there is a reduction wave at a lower potential in both electrolytes. Subsequent scans (see Fig. S5†) show that the reduction peak corresponds with a matching oxidation peak, consistent with decomposition of the AcPT radical cation into a new compound that displays a reversible oxidation. Dahn's report on phenothiazine-based

redox shuttles showed that AcPT initially protects at 2.4 V in an LTO/$LiFePO_4$ battery but drops during an overcharge cycle.[18,19] Based on this cycling data, we suggest that a decomposition product of the AcPT radical cation enables the large number of overcharge protection cycles.

In the second portion of our study, we generated solutions of redox shuttle radical cations from reaction with $TDBPA^{\bullet+}$ and monitored their lifetimes. For UV-vis studies, it is necessary to identify a consistent concentration of radical cation for all samples that does not saturate the instrument detector. A radical cation concentration of 3.0×10^{-4} M yielded initial spectra with absorption maxima of 2.5 or lower. The initial spectra, collected within 1 min of radical cation generation, are shown in Fig. 3a. Subsequent spectra of each radical cation are shown in Fig. 3b–f.

The absorption bands of the radical cations are red-shifted in comparison to their neutral counterparts, which have absorption maxima ranging from 280–380 nm. The most intense peak for the radical cation forms occurs between 420 and 550 nm, and all radical cations show less intense peaks at lower energies. Within each radical cation spectrum, the intensities of two peaks were monitored over time: (1) the tallest peak in the visible region (restricted to 400–600 nm) and (2) the tallest peak in the far red region (restricted to 700–1100 nm). In each figure, the monitored peaks are identified with a marker based on the trend in peak intensity: an arrow pointing down if the peak intensity decreases over time, an arrow pointing up if the peak intensity increases over time, and a line if the peak intensity does not change significantly. For comparison with battery electrolyte, both solvent alone and solvent with lithium salt, we generated radical cations in ethylene carbonate/ethyl methylcarbonate (EC/EMC, 3 : 7 ratio) with and without 1.2 M $LiPF_6$ (Fig. S7†). Radical cation spectra are nearly identical in all three solvents.

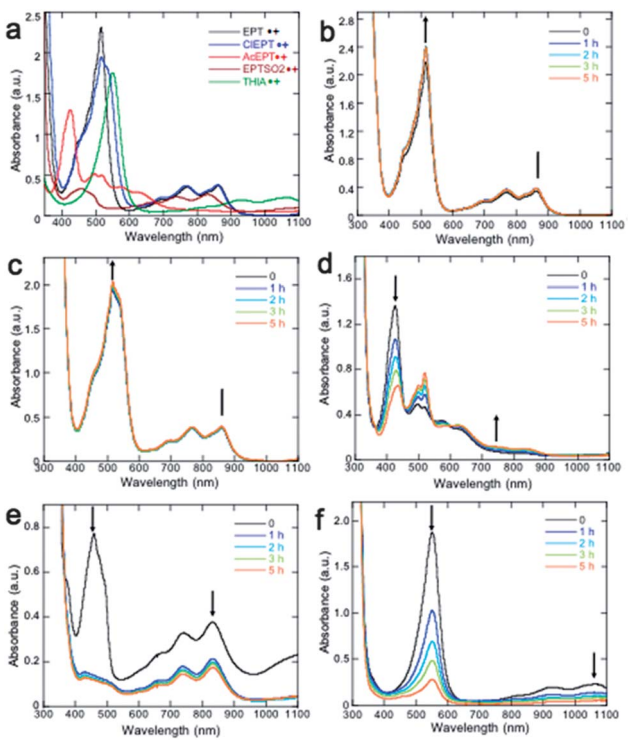

Fig. 3 UV-vis absorption spectra of the radical cations of previously reported redox shuttles at 0 min (A). Plots of the absorption spectra for radical cations $EPT^{\bullet+}$ (B), $ClEPT^{\bullet+}$ (C), $AcPT^{\bullet+}$ (D), $EPTSO2^{\bullet+}$ (E), and $THIA^{\bullet+}$ (F) at 0, 1, 2, 3, and 5 h.

The marked peaks in the spectra for EPT (Fig. 3b) and ClEPT (Fig. 3c) increase slowly with time. This can be explained by oxidation of a small portion of the excess neutral redox shuttle by DCM, which is prone to oxidizing aromatic compounds with low oxidation potentials. Otherwise the lack of significant change in the absorption spectra over time indicate a large number of overcharge protection cycles. The intensity of the peaks in the spectra of the radical cations of EPTSO2 (Fig. 3e) and THIA (Fig. 3f) decrease rapidly, indicating that these radical cations are unstable at this concentration in DCM, consistent with their relatively low number of cycles compared to that of the radical cations of EPT and ClEPT are stable at this concentration in DCM, consistent with their relatively large overcharge protection. The spectra of AcPT (Fig. 3d) are unique in that some peak intensities increase while others decrease with time. The change of the spectral shape over time is consistent with the formation of a new product that has transitions at similar energies as AcPT. Based on the UV-vis spectra, this product could be a new radical cation or a neutral compound with extended conjugation. For comparison, spectral changes were also monitored in EC/EMC and in 1.2 M $LiPF_6$ in EC/EMC (Fig. S8†) and showed similar trends in decay, the exception being the EPT radical cation in $LiPF_6$/EC/EMC, which increased in signal due to oxidation of excess neutral compound by the electrolyte salt.

While the UV-vis spectra are consistent with those reported for the same or similar compounds, analysis of the UV-vis spectra alone is not sufficient to confirm that a radical cation was generated. Even if the radical cation is formed, monitoring the intensity of a specific wavelength over time does not guarantee that the concentration of radical cation correlates linearly to the absorbance at that wavelength. For example, if a decomposition product forms that is not a radical, it may still have a peak with absorbance at the same wavelength. To unambiguously monitor the radical cation concentration, electron paramagnetic resonance (EPR) is necessary because an EPR signal is only observed if a radical is present. EPR spectra are plotted as a derivative, so it is necessary to integrate the spectrum twice to obtain the relative concentration of radical cation over time. The area under the doubly integrated spectrum can be used to measure the concentration of radical cation in comparison to samples of known concentration when spectra are collected using the same instrument parameters. We wanted to compare the trends in decay of the area under integrated EPR spectra to the peak monitored in the UV-vis spectrum to determine if UV-vis analysis gave the same results as measuring radical cation concentration.

For EPR measurements, radical cations were generated in DCM in a 10 : 1 ratio of neutral compound to oxidant, generating the spectra shown in Fig. 4a. All spectra were plotted with the same intensity scale[52] except for the radical cation of THIA.

Because the spectrum of the THIA radical cation is narrower than the other radical cations, the peaks in its spectrum are more intense. In Fig. 4b–e, the spectra for each radical cation are shown over time. It was not possible to record EPR spectra at r.t. in EC/EMC with or without $LiPF_6$ due to high dielectric constants of carbonates, so additional EPR spectra are not provided in battery electrolyte.

The triplet in the EPR spectra of $EPT^{\bullet+}$ and $ClEPT^{\bullet+}$ is consistent with coupling to one nitrogen atom, and have similar spectra in both cases. As the electronics of the ring system are altered with electron-withdrawing groups or by replacing heteroatoms in the aromatic ring, the shape of the spectra changes. In the EPR spectrum for $THIA^{\bullet+}$, in which there is no nitrogen atom, the signal is a singlet. The original EPR spectra shown in Fig. 4a show relatively strong signals for $EPT^{\bullet+}$, $ClEPT^{\bullet+}$, and $THIA^{\bullet+}$. For $AcPT^{\bullet+}$ and $EPTSO2^{\bullet+}$, however, the spectra are much less intense, with almost no measurable signal, indicating a low concentration of radical cation. The intensity of the $AcPT^{\bullet+}$ spectrum was unexpected based on the UV-vis results. Based on UV-vis alone, we had expected a relatively intense, stable EPR signal but instead had almost no signal. However, considering the tendency of the UV-vis spectra to change shape over time, it is likely that the $AcPT^{\bullet+}$ almost immediately decomposes into a new product that is not a radical cation. This explanation is consistent with the CV results, which show that the $AcPT^{\bullet+}$ rapidly decomposes into a new product with a lower oxidation potential than AcPT.

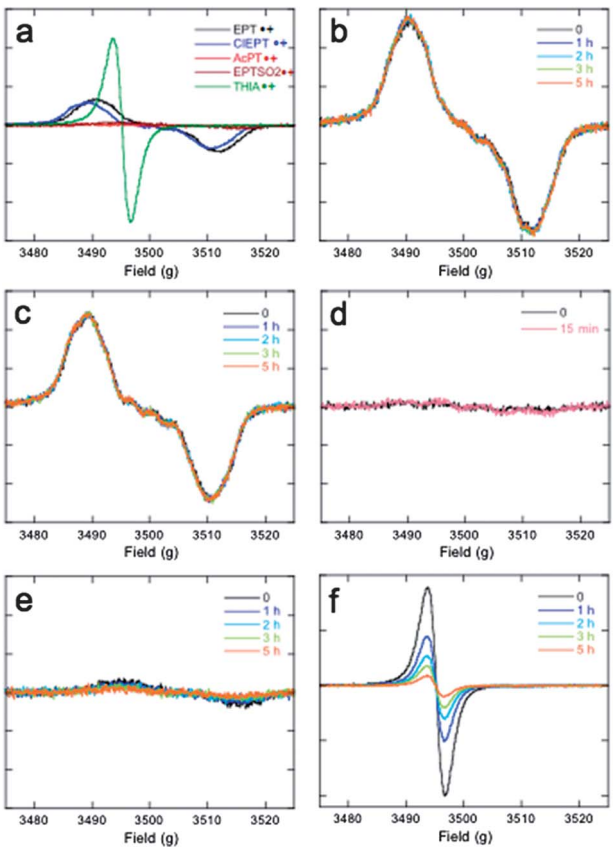

Fig. 4 EPR spectra of the radical cations of previously reported redox shuttles in DCM at 0 min (A) and the spectra for $EPT^{\bullet+}$ (B), $ClEPT^{\bullet+}$ (C), $AcPT^{\bullet+}$ (D), $EPTSO2^{\bullet+}$ (E), and $THIA^{\bullet+}$ (F) at 0, 1, 2, 3, and 5 h.

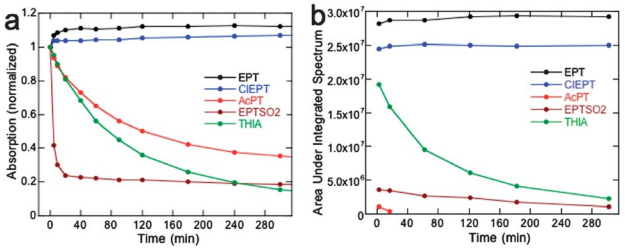

Fig. 5 Plot of the normalized maximum absorbance *vs.* time (a) and the area under integrated EPR spectrum *vs.* time (b) for $EPT^{\bullet+}$, $ClEPT^{\bullet+}$, $AcPT^{\bullet+}$, $EPTSO2^{\bullet+}$, and $THIA^{\bullet+}$ generated at 3.0×10^{-4} M in DCM from 0–5 h.

Except for the case of AcPT, the changes in EPR spectra over time were consistent with the UV-vis results. To quantify these changes and to compare the UV-vis and EPR results, we next generated two plots. For the UV-vis spectra, we took an average of the absorbance values of the tallest peak over three runs. Because the molar absorptivity of the tallest peak may be different for every radical cation, absorbance values do not necessarily correlate to radical cation concentration from one sample to another. Therefore we normalized the average absorbance of the first sample acquired to 1.0, dividing the remaining absorbance values for that radical cation by the same number used to normalize the initial absorbance. Thus, each value starts at a normalized absorbance of 1.0. We did not normalize the area under the EPR spectra because these values are unique to concentration of radical species and are not dependent on molecular properties. A plot of normalized absorbance *vs.* time is shown in Fig. 5a, and a plot of the area under the integrated EPR spectrum *vs.* time is shown in Fig. 5b (see Fig. S6† in the ESI for the UV-vis plot with error bars included, as well as a plot of the most intense peak in the far red region *vs.* time).

When comparing the plot of absorbance *vs.* time to the area under the integrated EPR spectrum *vs.* time, one can see many similarities. The values for $EPT^{\bullet+}$ and $ClPT^{\bullet+}$ are almost unchanging over time. $THIA^{\bullet+}$ has almost the same trend in both cases, and if one takes into account that the rapid decrease in $EPTSO2^{\bullet+}$ in the UV-vis spectrum may have occurred before the EPTSO2 sample can be tuned in the EPR cavity, the remaining values are low in intensity and show a slow rate of change. The major difference is that of $AcPT^{\bullet+}$. The UV-vis data do not discern that the changing absorbance values, while decreasing, are almost nonexistent in the EPR spectra. Therefore we propose a general guideline for analyzing UV-vis spectra of radical cations over time: if the shape of a UV-vis spectrum changes over time (some peaks increase in intensity while others decrease), then the change in absorbance intensity at any one wavelength is not useful for reliably predicting radical cation stability (Fig. 6). As long as we monitor not only the peak intensity, but consider also the shape of the spectrum over time, then we can rely on the UV-vis peak intensity to analyze radical cation stability.

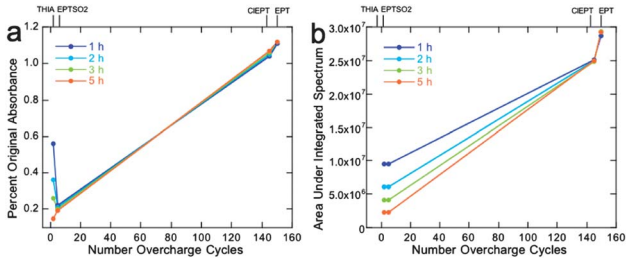

Fig. 6 Plot of percent of original absorbance for the tallest peak in the UV-vis spectrum (A) and plot of area under integrated EPR spectrum (B) in DCM, each *vs.* the number of overcharge cycles reported for THIA, EPTSO2, ClEPT, and EPT with $LiFePO_4$/LTO electrodes.

In order to know if these results are useful for predicting overcharge performance in LIBs, it is necessary to compare the values for absorbance (UV-vis) and area under the integrated spectra (EPR) at different times *vs.* the number of overcharge cycles reported for these derivatives.[17,18,45] Therefore plots were generated for 1, 2, 3, and 5 h for the UV-vis and EPR values *vs.* the number of overcharge cycles. Because we are confident that the $AcPT^{\bullet+}$ decomposes into at least one new material, we excluded it from this plot as we expect that our data will not lead to a reliable prediction in the case of AcPT. Here the values of the percent signal (absorbance or integrated area) of $EPT^{\bullet+}$, $ClEPT^{\bullet+}$, $EPTSO2^{\bullet+}$, and $THIA^{\bullet+}$ at 1 h, 2 h, 3 h, and 5 h are plotted *vs.* their number of overcharge cycles in coin cells with $Li_{4/3}Ti_{5/3}O_4$ and $LiFePO_4$ electrodes and 0.5 M LiBOB in propylene carbonate (PC)/dimethyl carbonate (DMC)/ethylene carbonate (EC)/diethyl carbonate (DEC) in a 1 : 2 : 1 : 2 ratio by volume as the electrolyte[17,18,45] (see Fig. S9† in the ESI for plots that include AcPT values).

The percent UV-vis absorbance and the area under the integrated EPR spectrum show that the redox shuttles having more stable radical cations correspond to a larger number of cycles of overcharge protection. The plot that is the most linear is the 5 h plot in the UV-vis in DCM experiment. Until 5 h in DCM, this method predicts that THIA and EPTSO2 are switched, but over time, THIA decays significantly and drops below EPTSO2. For the EPR spectra, the time required to tune the EPR cavity for each sample prevents us from differentiating between THIA and EPTSO2, but does correctly predict that ClEPT protects batteries from overcharge for a larger number of cycles than does EPT. Notably, while the stabilities of radical cations may vary significantly from one solvent to another, analysis of the radical cation stability in DCM as measured by UV-vis spectroscopy yielded the same trends as in battery electrolyte, both with and without the lithium salt.

IV. Conclusions

In conclusion, we have measured the stability of the radical cations of five related redox shuttles in dichloromethane using UV-vis and EPR spectroscopy. We found that monitoring the absorbance of the most intense peak in the UV-vis spectrum provided a correlation in radical cation stability *vs.* the number of overcharge cycles in LIBs. UV-vis and EPR yielded similar trends. In 5 h or less, we can predict which redox shuttles are the most stable and can weed out the poorer performing shuttles, as long as we note the appropriate exceptions, that include having a UV-vis spectrum that changes in shape over time; in which case we cannot expect to be able to predict redox shuttle performance. This relatively inexpensive method requires only the purchase of a diode array UV-vis spectrometer, anhydrous solvents, and reagents to prepare the chemical oxidant, which may make redox shuttle analysis accessible to more laboratories. DCM can be used instead of battery electrolyte, as results in both solvents show similar trends in decay. Despite the change in concentration and environment, our UV-vis and EPR studies in DCM show that radical cation stability provides an indication of redox shuttle performance in overcharging batteries, thus enabling laboratories containing standard synthetic organic supplies and instruments to study redox shuttle candidates without the purchase and assembly of supplies and equipment for battery testing. Our future work will be extended to testing additional series of related redox shuttles to determine if we can reliably use this method to predict redox shuttle performance in different classes of aromatic compounds. Additionally, we will compare our results to those obtained in battery electrolyte to determine the effect of solvent environment on trends in prediction.

Acknowledgements

Acknowledgement is made to the donors of the American Chemical Society Petroleum Research Fund for support (or partial support) of this research through a Doctoral New Investigator Award as well as the University of Kentucky's Office of the Vice President for Research and the College of Arts & Sciences for start-up funding. We thank Nelson Ng for his assistance in UV-vis studies and Corrine F. Elliott for her assistance in the synthesis of EPT.

References and Notes

1 B. Dunn, H. Kamath and J. M. Tarascon, *Science*, 2011, **334**, 928–935.
2 J. M. Tarascon and M. Armand, *Nature*, 2001, **414**, 359–367.
3 P. Yang and J. M. Tarascon, *Nat. Mater.*, 2012, **11**, 560–563.
4 J. Wen, Y. Yu and C. Chen, *Mater. Express*, 2012, **2**, 197–212.
5 J. B. Goodenough and Y. Kim, *Chem. Mater.*, 2009, **22**, 587–603.
6 P. Ribiere, S. Grugeon, M. Morcrette, S. Boyanov, S. Laruelle and G. Marlair, *Energy Environ. Sci.*, 2012, **5**, 5271–5280.
7 M. Armand and J. M. Tarascon, *Nature*, 2008, **451**, 652–657.
8 Z. Chen, Y. Qin and K. Amine, *Electrochim. Acta*, 2009, **54**, 5605–5613.
9 J. N. Reimers and J. R. Dahn, *J. Electrochem. Soc.*, 1992, **139**, 2091–2097.
10 K. Kumai, H. Miyashiro, Y. Kobayashi, K. Takei and R. Ishikawa, *J. Power Sources*, 1999, **81-82**, 715–719.

11 D. P. Abraham, E. P. Roth, R. Kostecki, K. McCarthy, S. MacLaren and D. H. Doughty, *J. Power Sources*, 2006, **161**, 648–657.
12 W. Kong, H. Li, X. Huang and L. Chen, *J. Power Sources*, 2005, **142**, 285–291.
13 K. M. Abraham, D. M. Pasquariello and E. B. Willstaedt, *J. Electrochem. Soc.*, 1990, **137**, 1856–1857.
14 M. N. Golovin, D. P. Wilkinson, J. T. Dudley, D. Holonko and S. Woo, *J. Electrochem. Soc.*, 1992, **139**, 5–10.
15 G. Halpert, S. Surampudi, D. Shen, C. K. Huang, S. Narayanan, E. Vamos and D. Perrone, *J. Power Sources*, 1994, **47**, 287–294.
16 F. Tran-Van, M. Provencher, Y. Choquette and D. Delaboughlise, *Electrochim. Acta*, 1999, **44**, 2789–2792.
17 C. Buhrmester, J. Chen, L. Moshurchak, J. Jiang, R. L. Wang and J. R. Dahn, *J. Electrochem. Soc.*, 2005, **152**, A2390–A2399.
18 C. Buhrmester, L. Moshurchak, R. L. Wang and J. R. Dahn, *J. Electrochem. Soc.*, 2006, **153**, A228–A294.
19 The potential at which overcharge occurs is consistent with the oxidation potential of AcPT *vs.* $Li^{+/0}$; the overcharge potential is calculated based on the potential difference between LTO (the anode) and $Li^{+/0}$.
20 J. Chen, C. Buhrmester and J. R. Dahn, *Electrochem. Solid-State Lett.*, 2005, **8**, A59–A62.
21 Z. Chen, J. Liu, A. N. Jansen, G. GirishKumar, B. Casteel and K. Amine, *Electrochem. Solid-State Lett.*, 2010, **13**, A39–A42.
22 J. R. Dahn, J. Jiang, L. M. Moshurchak, M. D. Fleishchauer, C. Buhrmester and L. J. Krause, *J. Electrochem. Soc.*, 2005, **152**, A1283–A1289.
23 L. M. Moshurchak, C. Buhrmester and J. R. Dahn, *J. Electrochem. Soc.*, 2008, **155**, A129–A131.
24 L. M. Moshurchak, W. M. Lamanna, M. Bulinski, R. L. Wang, R. R. Garsuch, J. Jiang, D. Magnuson, M. Triemert and J. R. Dahn, *J. Electrochem. Soc.*, 2009, **156**, A309–A312.
25 Z. Zhang, L. Zhang, J. A. Schlueter, P. C. Redfern, L. Curtiss and K. Amine, *J. Power Sources*, 2010, **195**, 4957–4962.
26 L. Zhang, Z. Zhang, H. Wu and K. Amine, *Energy Environ. Sci.*, 2011, **4**, 2858–2862.
27 L. Zhang, Z. Zhang, P. C. Redfern, L. A. Curtiss and K. Amine, *Energy Environ. Sci.*, 2012, **5**, 8204–8207.
28 W. Weng, Z. Zhang, P. C. Redfern, L. A. Curtiss and K. Amine, *J. Power Sources*, 2011, **196**, 1530–1536.
29 G. Chen and T. J. Richardson, *Electrochem. Solid-State Lett.*, 2004, **7**, A23–A26.
30 L. Xiao, X. Ai, Y. Cao and H. Yang, *Electrochim. Acta*, 2004, **49**, 4189–4196.
31 J. K. Feng, X. P. Ai, Y. L. Cao and H. X. Yang, *J. Power Sources*, 2006, **161**, 545–549.
32 G. Chen and T. J. Richardson, *J. Electrochem. Soc.*, 2010, **157**, A735–A740.
33 B. Wang, T. J. Richardson and G. Chen, *Phys. Chem. Chem. Phys.*, 2013, **15**, 6849–6855.
34 C. Buhrmester, L. M. Moshurchak, R. L. Wang and J. R. Dahn, *J. Electrochem. Soc.*, 2006, **153**, A1800–A1804.
35 L. M. Moshurchak, C. Buhrmester, R. L. Wang and J. R. Dahn, *Electrochim. Acta*, 2007, **52**, 3779–3784.
36 G. GirishKumar, W. H. Bailey, B. K. Peterson and W. J. Casteel, *J. Electrochem. Soc.*, 2011, **158**, A146–A153.
37 W. K. Behl and D. T. Chin, *J. Electrochem. Soc.*, 1988, **135**, 16–21.
38 W. K. Behl and D. T. Chin, *J. Electrochem. Soc.*, 1988, **135**, 21–26.
39 W. K. Behl, *J. Electrochem. Soc.*, 1989, **136**, 2305–2310.
40 M. Schmittel and A. Burghart, *Angew. Chem., Int. Ed. Engl.*, 1997, **36**, 2550–2589.
41 M. A. Ischay and T. P. Yoon, *Eur. J. Org. Chem.*, 2012, **2012**, 3359–3372.
42 J. Roncali, *Chem. Rev.*, 1992, **92**, 711–738.
43 P. Audebert and P. Hapiot, *Synth. Met.*, 1995, **75**, 95–102.
44 B. Fabre, K. Michelet, N. Simonet and J. Simonet, *J. Electroanal. Chem.*, 1997, **425**, 67–75.
45 R. L. Wang and J. R. Dahn, *J. Electrochem. Soc.*, 2006, **153**, A1922–A1928.
46 Z. Chen, Q. Wang and K. Amine, *J. Electrochem. Soc.*, 2006, **153**, A2215–A2219.
47 L. Moshurchak, C. Burhmester and J. R. Dahn, *J. Electrochem. Soc.*, 2005, **152**, A1279–A1282.
48 S. K. Lee, M. J. Cho, H. Yoon, S. H. Lee, J. H. Kim, Q. Zhang and D. H. Choi, *Macromol. Res.*, 2004, **5**, 484–489.
49 W. Schmidt and E. Steckhan, *Chem. Ber.*, 1980, **113**, 577–585.
50 Y. Murata, F. Cheng, T. Kitagawa and K. Komatsu, *J. Am. Chem. Soc.*, 2004, **126**, 8874–8875.
51 Lone pair electrons are shown only on the nitrogen atoms. Note that while the reaction is drawn as an electron transfer from one nitrogen atom to another, the charge can be delocalized throughout the π bonds and lone pair electrons participating in resonance.
52 A *y*-axis is not shown in the EPR spectra because the units are arbitrary.